Article

Must the Best Laboratory Prepared Catalyst Also Be the Best in an Operational Application?

Lucie Obalová [1,*] , **Anna Klegova** [1] , **Lenka Matějová** [1] , **Kateřina Pacultová** [1]
and **Dagmar Fridrichová** [1,2]

1   Institute of Environmental Technology, VŠB – Technical University of Ostrava, 17. listopadu 15/2172,
    708 00 Ostrava, Czech Republic; anna.klegova@vsb.cz (A.K.); lenka.matejova@vsb.cz (L.M.);
    katerina.pacultova@vsb.cz (K.P.); dagmar.fridrichova@vsb.cz (D.F.)
2   Centre ENET, VŠB – Technical University of Ostrava, 17. listopadu 15/2172, 708 00 Ostrava, Czech Republic
*   Correspondence: lucie.obalova@vsb.cz

check for
updates

Abstract: Three cobalt mixed oxide deN$_2$O catalysts, with optimal content of alkali metals (K, Cs), were prepared on a large scale, shaped into tablets, and tested in a pilot plant reactor connected to the bypassed tail gas from the nitric production plant, downstream from the selective catalytic reduction of NO$_x$ by ammonia (SCR NO$_x$/NH$_3$) catalyst. High efficiency in N$_2$O removal (N$_2$O conversion of 75–90% at 450 °C, VHSV = 11,000 m^3 m$_{bed}$$^{-3}$ h^{-1}) was achieved. However, a different activity order of the commercially prepared catalyst tablets compared to the laboratory prepared catalyst grains was observed. Catalytic experiments in the kinetic regime using laboratory and commercial prepared catalysts and characterization methods (XRD, TPR-H$_2$, physisorption, and chemical analysis) were utilized to explain this phenomenon. Experimentally determined internal effectiveness factors and their general dependency on kinetic constants were evaluated to discuss the relationship between the catalyst activity in the kinetic regime and the internal diffusion limitation in catalyst tablets as well as their morphology. The theoretical N$_2$O conversion as a function of the intrinsic kinetic constants and diffusion rate, expressed as effective diffusion coefficients, was evaluated to estimate the final catalyst performance on a large scale and to answer the question of the above article title.

Keywords: internal effectiveness factor; effective diffusion coefficient; N$_2$O; catalytic decomposition; cobalt mixed oxide; alkali metal; promoter

1. Introduction

Research of new catalysts for industrial application is a time-consuming and costly process. It is usually based on a large number of laboratory catalytic experiments, which provide feedback for the optimization of catalyst preparation procedure, its chemical and phase composition, morphology, dispersion, and a number of other physicochemical characteristics which are necessary to obtain the desired catalytic properties. The result of laboratory research is the recipe for preparation of the optimized catalyst on a larger scale (approx. 100 kg), its production, and pilot plant testing.

In the presented work, based on previous extensive laboratory screening tests of N$_2$O catalytic decomposition [1–3], three cobalt mixed oxide deN$_2$O catalysts with optimal content of alkali metals K/Co$_4$MnAlO$_x$, Cs/Co$_4$MnAlO$_x$, and Cs/Co$_3$O$_4$ were prepared on a large scale, shaped into tablets and tested in the pilot plant reactor connected to the bypassed tail gas from the nitric production plant. Results of pilot plant testing of K/Co$_4$MnAlO$_x$ for decreasing N$_2$O emissions from a nitric acid plant were published in our previous work [4]. Although high efficiency in N$_2$O removal (N$_2$O conversion of 75–90% at 450 °C, VHSV = 11,000 m^3 m$_{bed}$$^{-3}$ h^{-1}) were reached; the question is if the prepared tablet catalyst achieved similar catalytic performance to the laboratory catalyst or if it was lower and

in the latter case optimization of the pilot catalyst's preparation procedure would then be beneficial. The same question applies in the case of the remaining two catalysts. For Cs/Co_4MnAlO_x, the results of pilot plant testing were published in [5] and for Cs/Co_3O_4 catalyst, the pilot-testing results have not yet been published.

The aim of this paper is to answer the question already posed in the title. Catalytic experiments in kinetic regime using laboratory and commercial prepared catalysts and characterization methods (XRD, TPR-H_2, physisorption and chemical analysis) were utilized to answer this question. The procedure for determination of (i) the effective diffusion coefficients from catalytic experiments and (ii) the theoretical limits of catalyst performance on a large scale is shown. The presented approach is generally valid and can be used also for other reactions of 1st order kinetics.

2. Results

2.1. N_2O Catalytic Decomposition

Figure 1 compares the laboratory and pilot-plant results of N_2O catalytic decomposition. Laboratory experiments were performed using laboratory-prepared catalysts in the form of grains and the conversion of N_2O was observed in a gaseous mixture simulating real waste gas conditions. Pilot-plant experiments were performed on commercially prepared tablets in real tail-gas from a nitric acid plant. High efficiencies in N_2O removal in both laboratory and pilot-plant conditions were reached, comparable with the best results from the literature [6,7].
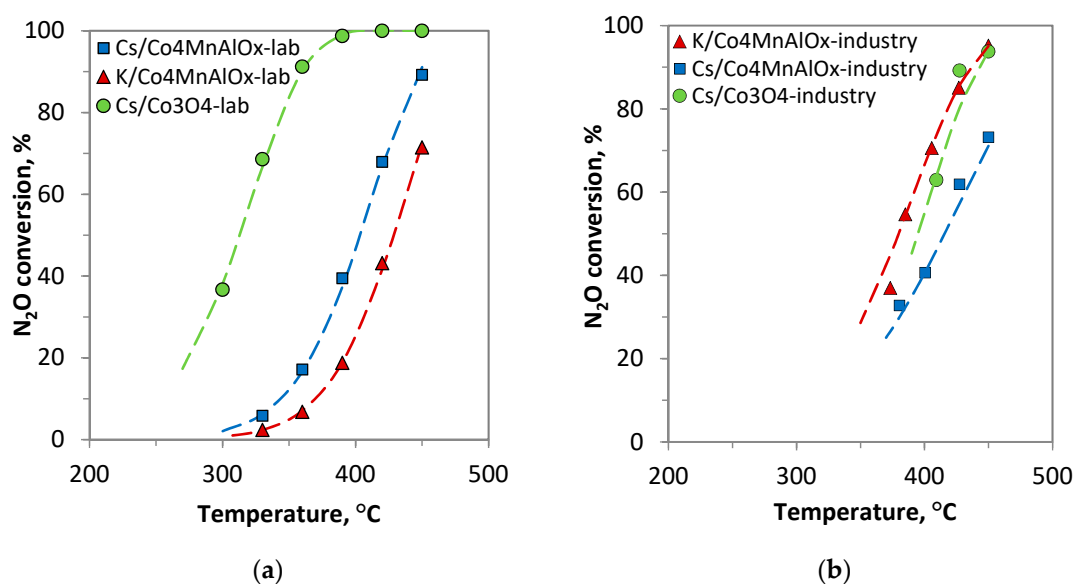

(a)   (b)

Figure 1. N_2O catalytic decomposition over: (**a**) laboratory prepared catalyst grains in simulated process condition (1000 ppm N_2O + 5 mol% O_2 + 2 mol% H_2O in N_2, GHSV = 60,000 l kg^{-1} h^{-1}); (**b**) commercially prepared catalyst tablets in real waste gas (VHSV = 11,000 m^3 m_{bed}^{-3} h^{-1}, real waste gas (512 ± 135 ppm N_2O, 26 ± 16 ppm NO_x, 9 ± 3 ppm NH_3, $p = 0.6$ MPa). Points—experimental data; dashed line—model (Equation (2)).

As expected, the conversions achieved under laboratory and pilot-plant conditions vary due to different composition of the gaseous mixture, space velocities, pressure, and the effect of internal diffusion inherent to the use of commercial tablets. However, the order of catalysts' activities reached under laboratory and pilot-plant conditions also changed, which was unexpected. The highest N_2O conversions under laboratory conditions were achieved using the Cs/Co_3O_4 catalyst, but under pilot-plant conditions, comparable N_2O conversions were obtained over the K/Co_4MnAlO_x catalyst, which was the worst performing under laboratory conditions.

Three questions arise:

1. What are the reasons for the different activity order of commercially prepared catalyst tablets compared to laboratory-prepared samples?
2. Could our pilot-plant catalysts achieve higher activity (N_2O conversions)?
3. What are the theoretical limits of N_2O conversions over catalyst tablets and how to approach them?

To answer the first question, catalytic experiments with commercially prepared tablets were carried out under laboratory conditions in simulated tail-gas (Figure 2). It is evident that the order of catalytic activities of commercial tablets was quite different to that in real waste gas (Figure 1b) but the same as for laboratory prepared catalysts tested in kinetic regime (Figure 1a). It is therefore implied that the different order of catalytic activities in the pilot-plant experiment (Figure 1b) was caused by the different conditions of the said experiment, particularly by the presence of NO_x gases, although their concentration was quite low (max 26 ppm). Significant inhibition of N_2O decomposition caused by NO_x in the presence of cobalt catalysts modified by alkali promoters was previously reported [2,8,9]. The extent of the inhibiting effect depends on the alkali promoter type and its amount. The real tail gas also contained residual NH_3. The effect of NH_3 on the decomposition of N_2O in the presence of cobalt catalysts was studied only sporadically; mainly on zeolites and to a lesser extent on oxidic catalysts [10,11]. The influence of NH_3 in the feed gas was also studied in an individual experiment performed under laboratory conditions over K/Co_4MnAlO_x-industry tablets [4]. It was found that ammonia oxidized to N_2O, NO, NO_2, and probably N_2 (not measured), which means that ammonia can also contribute to the fluctuations of NO_x concentration present in the feed or can also increase N_2O concentration at the reactor outlet. Laboratory and pilot-plant experiments were also performed under different pressures. Pilot-plant experiments were performed at higher pressure, which has a positive effect on the N_2O catalytic decomposition rate [12].
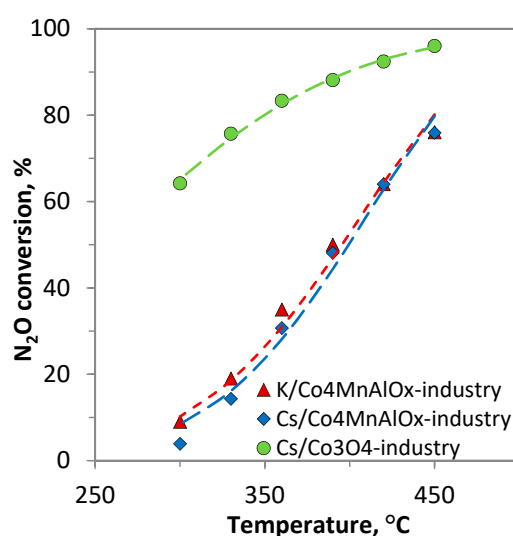

Figure 2. N_2O catalytic decomposition over industrially prepared catalysts (tablets 5 mm $\times$ 5 mm) tested in laboratory conditions. Points—experimental data; dashed line—model (Equation (2)). Conditions: VHSV = 3000 m^3 m_{bed}^{-3} h^{-1}, 1000 ppm N_2O + 5 mol% O_2 + 2 mol% H_2O in N_2.

To answer the second question, N_2O decomposition was carried out in kinetic regime on laboratory and commercially prepared catalysts in grain form (Figure 3). First order kinetic constants using an ideal plug flow reactor model were also determined according to Equation (3), both for data in Figure 3a–c (grain catalysts) and for data in Figure 2 (tablet catalysts). Reaction rates (Equation (5)) and internal effectiveness factors (Equation (1)) were determined. A summary of the calculated kinetic parameters is shown in Table 1.
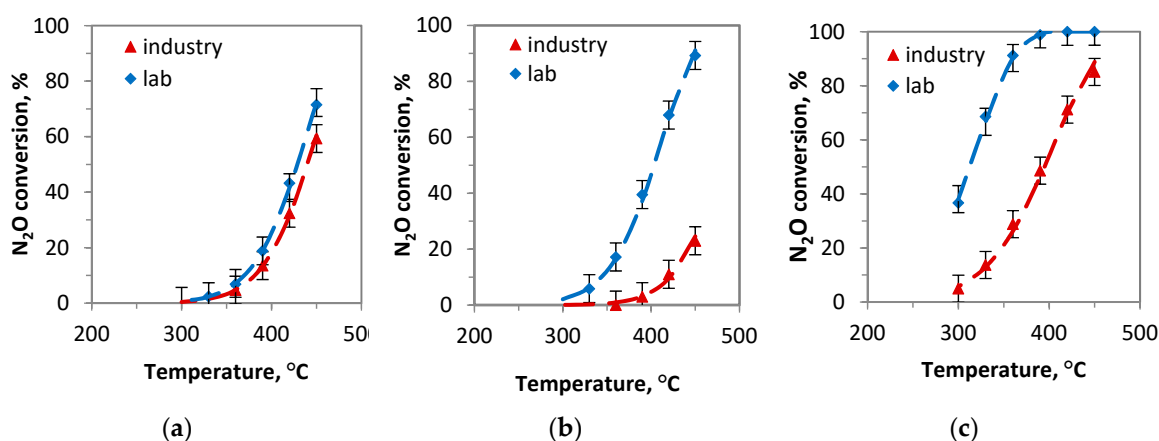
Figure 3. N₂O decomposition over laboratory and commercially prepared catalysts in grain form: (**a**) K/Co_4MnAlO_x; (**b**) Cs/Co_4MnAlO_x; (**c**) Cs/Co_3O_4. Points—experimental data; dashed line—model (Equation (2)). Conditions: 1000 ppm N_2O + 5 mol% O_2 + 2 mol% H_2O in N_2, GHSV = 60,000 l kg^{-1} h^{-1}.

Table 1. Kinetic constants and reaction rates of N_2O catalytic decomposition over laboratory (grain form) and commercially prepared (grain and pellet forms) catalysts and estimated internal effectiveness factors. Conditions: 1000 ppm N_2O + 5 mol% O_2 + 2 mol% H_2O in N_2, 390 °C.

Parameter/Catalyst	K/Co_4MnAlO_x		Cs/Co_4MnAlO_x		Cs/Co_3O_4	
	Lab	**Industry**	**Lab**	**Industry**	**Lab**	**Industry**
k_{grain} (m³ kg⁻¹s⁻¹) × 10³	3.47	2.42	8.38	0.51	73.15	11.09
k_{grain}* (s⁻¹) × 10⁶ [1]	1.51	1.05	3.54	0.22	28.24	4.28
k_{pellet} (m³ kg⁻¹ s⁻¹) × 10³	-	0.47	-	0.37	-	1.32
r_{grain} (mol kg⁻¹h⁻¹) × 10²	-	3.37	-	0.75	-	12.12
r_{pellet} (mol kg⁻¹ h⁻¹) × 10²	-	0.70	-	0.55	-	1.90
η (-) [2]	-	0.21	-	0.73	-	0.15

[1] 1st order kinetic constant (s⁻¹) determined according to Equation (4)　[2] Calculated as $\eta = r_{grain}/r_{pellet}$ for commercially prepared catalysts

By comparing N_2O conversions, the values of X_A for the laboratory and commercially prepared K/Co_4MnAlO_x catalyst differ only by 12% maximum, at lower temperature the differences were within the margin of experimental error. This implies that the activity of active sites on the K/Co_4MnAlO_x-industry catalyst is nearly the same as on the laboratory prepared sample, K/Co_4MnAlO_x-lab and the reaction rate and kinetic constants of the tablet catalyst is lower mainly due to the inhibiting effect of internal diffusion. The main way to improve N_2O conversion is therefore to increase the internal effectiveness factor, which in this case has a value of 0.21. The possibilities of increasing the internal effectiveness factor are discussed in Chapter 3.

The situation is different with the Cs/Co_4MnAlO_x and Cs/Co_3O_4 catalysts. The N_2O conversion and kinetic constants in kinetic regime (k_{grain}) are significantly lower when comparing the commercial and laboratory prepared samples. In the case of Cs/Co_3O_4, the kinetic constant of the commercially prepared sample is six times lower and in the case of Cs/Co_4MnAlO_x 16 times lower. This implies that the sites on the surface of commercially prepared catalysts are less active than those on the surface of laboratory prepared catalysts. The kinetic constants k_{pellet} are lower than k_{grain} of laboratory prepared samples due to the effect of internal diffusion and another effect, which caused the activity decrease of active sites. The N_2O conversion using commercial tablets could be improved both by increasing the internal effectiveness factor and by increasing the activity of active sites to the same level as laboratory-prepared catalysts. It is important to note that by increasing activity, the internal effectiveness factor will decrease because parameters η and k are related to each other according to

Equation (6)–(8). To determine the cause of different activities of Cs/Co_4MnAlO_x and Cs/Co_3O_4 catalysts, a basic characterization of laboratory and commercially prepared catalysts was performed.

2.2. Physicochemical Properties of Catalysts

　　Basic physicochemical properties of laboratory and commercially prepared catalysts are shown in Table 2. Analysis of chemical composition shows that the molar ratio of Co:Mn:Al is basically the same for laboratory and commercially prepared Co_4MnAlO_x samples modified by K and Cs and is close to the ratio of 4:1:1, which was the aim during synthesis.

Table 2. Physicochemical properties of laboratory and commercially prepared catalysts.

		K/Co_4MnAlO_x		Cs/Co_4MnAlO_x		Cs/Co_3O_4	
		Industry	**Lab**	**Industry**	**Lab**	**Industry**	**Lab**
Chemical composition (wt%)	Co	45	49.6	45.7	46.0	63.4	68.0
	Mn	9.3	13.3	8.5	10.6	-	-
	Al	5.2	8.9	5.1	n.d.	-	-
	K/Cs	1.3	1.8	3.4	3.5	1.0	1.0
	Na	0.1	0.1	0.1	0.5	n.d.	0.04
Co:Mn:Al mol. ratio		4 : 0.7 : 0.7	4 : 1.2 : 1.6	4 : 0.9 : 1.0	4 : 1 : n.d.	-	-
S_{BET} (m^2/g)		93	98	68	86	20	13
r (nm) [1]		3.8	12.3	5.3	7.1	10.2	13.5
Alkali metal normalized loading (atoms/nm^2) [2]		1.9	2.8	2.1	1.8	2.4	3.5
Phase composition		Spinel, graphite	Spinel	Spinel, graphite	Spinel	Spinel, graphite	Spinel
L_c (nm)		9	7	13	7	18	49
a (nm)		0.8118	0.8110	0.8111	0.8116	0.8084	0.8086
T_{max} (°C) [3]		272; 377	320; 361	284; 390	168; 274; 359	352; 389	370
H_2 (mmol/g) [4]		4.5	4.8	4.2	4.1	14	12.9

[1] Mean pore radius $r = 2V/A$, where V is pore volume and A specific surface area S_{BET} [2] Calculated as K or Cs atoms/nm^2 [3] Temperature of reduction peak maxima from TPR-H_2 [4] H_2 consumption in 25–450 °C temperature interval from TPR-H_2

　　For catalytic activity, the content of alkali promoters is important [2,13,14]. The amount of Cs in laboratory and commercially prepared samples is the same and close to the optimal value of 3.5wt% for Co_4MnAlO_x [1] and 1wt% for Co_3O_4 [3]. In the case of K/Co_4MnAlO_x, the intention was to prepare the commercial catalyst with K content of 1.8wt%, which proved to be the most active in our previous work [2]. Here it was found that the optimal K content (determined by atomic emission spectroscopy, AES) leading to the highest N_2O conversion was 0.9–1.6wt% K in an inert gas and 1.6–2.8wt% K in the presence of O_2 and H_2O. The analysis of K content in a commercially prepared sample showed a lower K content, probably due to inhomogeneity, which is a known disadvantage of the impregnation method. All catalysts contained sodium residuals (0.04–0.50wt%) from the preparation procedure. Since our recent results showed that to affect catalytic activity, significantly higher Na content (>1.15 wt%) is necessary [8], we do not expect residual sodium to influence catalytic activity.

　　The comparison of the specific surface areas of laboratory and commercially prepared samples (Table 2) shows that, in terms of specific surface area, the transfer of catalyst synthesis to a larger scale was successful. Catalyst synthesis on a larger commercial scale led to a lower mean pore size for all three catalysts, which was caused by the use of high pressure during tabletization [15]. It was found out that on increasing pressure (up to 10 MPa) during tabletization of the catalyst matter (grains of defined size), the diameter of mesopores decreased, while the specific surface area stayed constant up to 8 MPa.

Measured nitrogen adsorption–desorption isotherms of commercially prepared catalysts (Figure 4a) indicate that there is a big difference between the individual samples. While the isotherms of K/Co_4MnAlO_x-industry and Cs/Co_4MnAlO_x-industry correspond to the mesoporous material with generally larger mesopores, the isotherm of Cs/Co_3O_4 corresponds to macroporous material. Comparing K/Co_4MnAlO_x-industry and Cs/Co_4MnAlO_x-industry samples, K/Co_4MnAlO_x-industry possesses smaller mesopores than Cs/Co_4MnAlO_x-industry (Figure 4b) which is at comparable total pore volumes reflected by the higher specific surface area of the pores of K/Co_4MnAlO_x-industry.
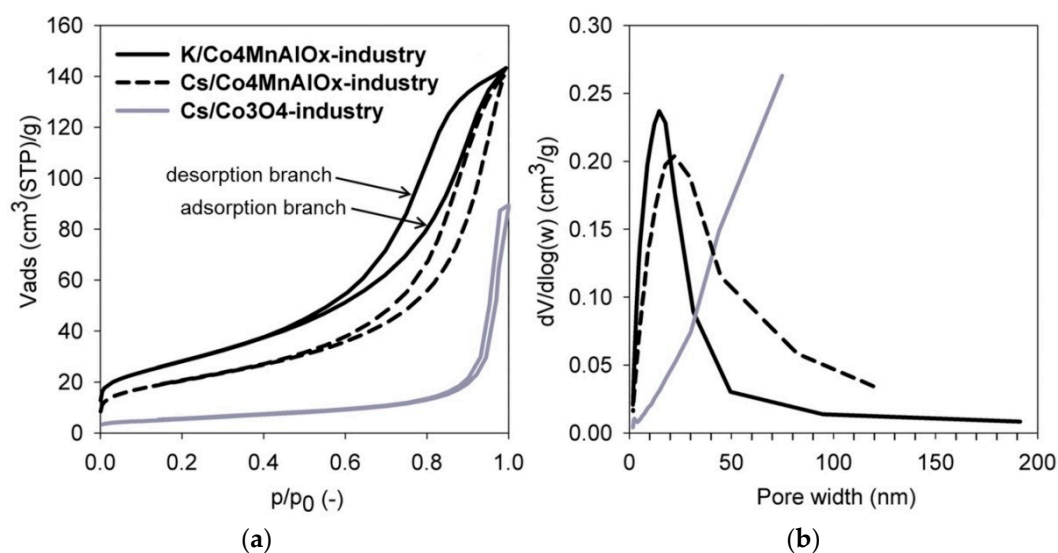

(a)   (b)

Figure 4. (**a**) Measured nitrogen adsorption–desorption isotherms and (**b**) evaluated pore-size distributions of commercially prepared catalysts.

All commercially prepared samples do not possess any micropores, thus, the values of the micropore volume and mesopore surface area are not shown in Table 3. The determined textural properties of the commercially prepared catalysts are summarized in Table 3.

Table 3. Textural properties of commercially prepared catalysts.

Catalyst	S_{BET} (m^2/g)	V_{net} (cm^3_{liq}/g)	Pore width$_{max}$ (nm)	ρ_c $(kg\ m^{-3})$	ε_p (-)
K/Co_4MnAlO_x-industry	101	0.220	15	2300	0.48
Cs/Co_4MnAlO_x-industry	73	0.217	22	2370	0.50
Cs/Co_3O_4-industry	19	0.138	above 75	2590	0.47

Results of phase composition are summarized in Figure 5 and Table 2. Measured diffraction lines characteristic for a cobalt spinel structure were indexed within the *Fd3m* space group and this structure was confirmed in all investigated samples as the major phase. Graphite was also found as a minor phase in all industrially prepared catalysts, together with the spinel phase, since graphite was added to the catalyst matter for ease of forming. Graphite line was not observed in the catalysts used in the long-term pilot plant testing (not shown here), confirming combustion of graphite during the catalytic test [4]. Small un-labelled diffractions correspond to the Kbeta line of the used *X*-ray radiation source. All Co_4MnAlO_x samples have slightly higher values of cell parameters (*a*) in comparison to pure Co_3O_4 due to incorporation of Mn and Al ions into the spinel structure. In addition, samples with Co_4MnAlO_x active phase have nanocrystalline structure and higher surface area in comparison to samples with Co_3O_4. Crystallite sizes (expressed as mean coherent domain size L_c) correlate with the determined surface area; the smaller the crystallite size the larger is the surface area. Potassium doped samples K/Co_4MnAlO_x-lab and -industry exhibit approximately similar size for coherent domain and

surface area. In the case of cesium doped Cs/Co_4MnAlO_x samples, the laboratory prepared catalyst has a less crystalline structure and higher surface area in comparison with the commercially prepared sample. Laboratory prepared cesium doped cobalt oxide Cs/Co_3O_4 exhibits the highest value of coherent domain size and the lowest specific surface area of all tested samples.
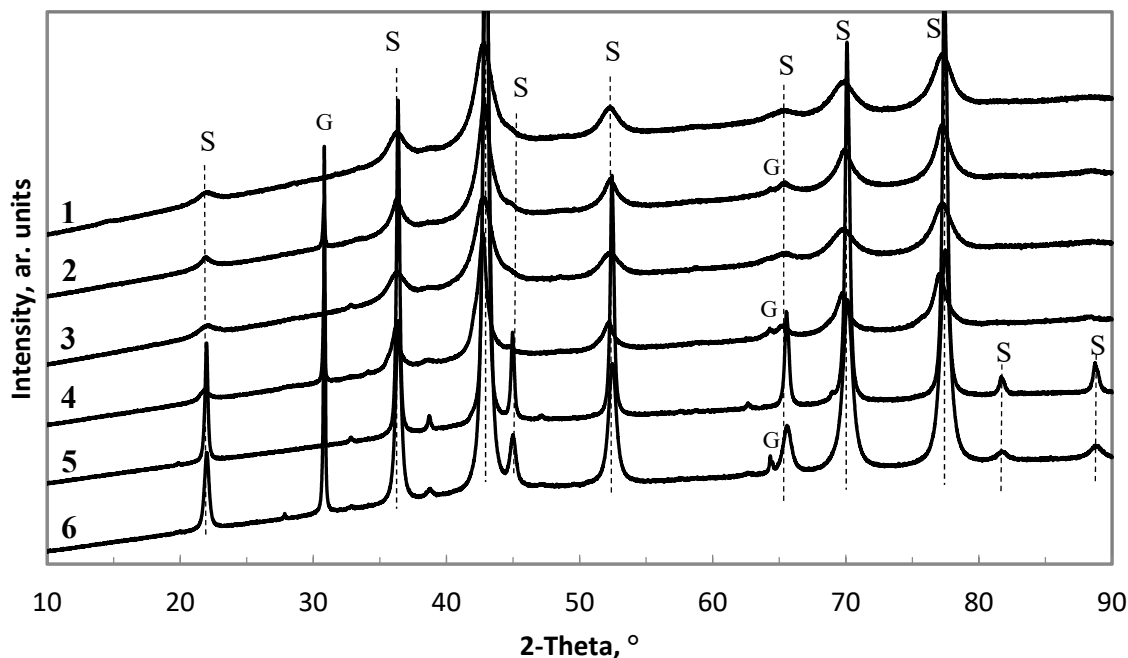

Figure 5. XRD patterns of the laboratory and commercially prepared catalysts: (**1**) K/Co_4MnAlO_x-lab; (**2**) K/Co_4MnAlO_x-industry; (**3**) Cs/Co_4MnAlO_x-lab; (**4**) Cs/Co_4MnAlO_x-industry; (**5**) Cs/Co_3O_4-lab; (**6**) Cs/Co_3O_4-industry. Phase designation: S—spinel, G—graphite.

The reduction patterns of catalysts prepared commercially and in the laboratory are shown in Figure 6. Since the catalytic reaction proceeds up to 450 °C, only species reducible in this temperature region (low temperature region) can contribute to the catalyst activity and for that reason only the low temperature area of TPR-H_2 is shown. For samples containing only cobalt species (besides alkali promoter), the main reduction peak can be ascribed to the reduction of $Co^{III} \rightarrow Co^{II} \rightarrow Co^0$. In the case of Cs/Co_3O_4, both reduction processes overlap (more for the laboratory prepared catalyst), suggesting not only different primary particle size but also different shapes of cobalt spinel nanocrystals [16]. The catalysts containing cobalt, manganese, and aluminum are reduced in two main temperature regions, 200–430 °C and >430 °C. Both reduction peaks consist of overlapping peaks corresponding to the reduction of more species. The low-temperature reduction peak also represents, besides the reduction of cobalt species in a segregated Co_3O_4-like phase, the reduction of Mn^{IV} to Mn^{III} oxides, while $Mn^{III} \rightarrow Mn^{II}$ reduction can take place in both temperature regions [17]. The high temperature peak was attributed to the reduction of Co and Mn ions surrounded by Al ions in the spinel-like phase [8]. The presence of alkali metals in the mixed oxides caused the formation of an easily reducible species (Co and/or Mn) manifested as a low temperature shoulder visible especially in Co_4MnAlO_x containing samples.

The quantitative data (Table 2) confirmed a comparable amount of reducible species (in the temperature range of 25–450 °C) in samples prepared commercially and in laboratory conditions, while samples containing only Co_3O_4 active phase possessed higher amounts of reducible components in comparison with Co_4MnAlO_x containing samples. The TPR profile shapes are similar for the relevant samples prepared commercially and in the laboratory; only small shifts are seen—the biggest changes are visible for Cs/Co_4MnAlO_x where the commercially prepared catalyst exhibits inferior reducibility. Since the reducibility of the cobalt and manganese species is affected by the primary particle size [18],

the visible changes are probably connected with different crystallite sizes as was also proved by the XRD results and the inhomogeneity of samples rather than a different chemico-electronic environment.
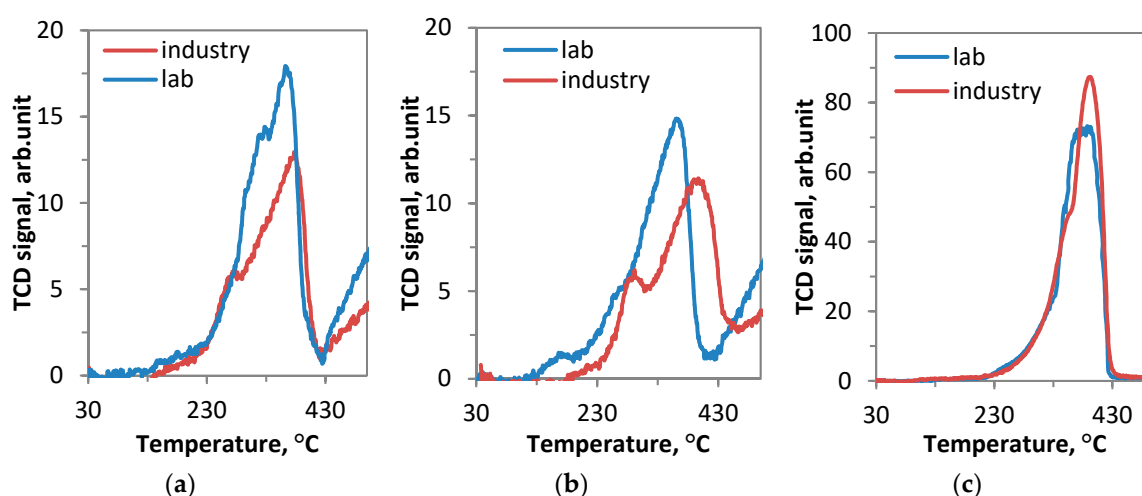

Figure 6. TPR-H_2 of the laboratory and commercially prepared catalysts: (**a**) K/Co_4MnAlO_x; (**b**) Cs/Co_4MnAlO_x; (**c**) Cs/Co_3O_4.

Published results imply that normalized loading of alkali metals (atoms/nm^2) on the catalyst surface is an important parameter of cobalt-based catalysts [19,20]. The reason is the electronic nature of the potassium and cesium promotion effect based on the formation of surface dipoles influencing the electron density of cobalt and manganese cations, which was confirmed by the direct correlation between N_2O conversion and surface work function catalysts [19]. Figure 7 shows the dependence of N_2O conversion on the normalized loading of K and Cs over Co_4MnAlO_x and Co_3O_4, utilizing data on the optimization of K [2] and Cs [1] content in Co_4MnAlO_x mixed oxide and Cs content in Co_3O_4 [3].
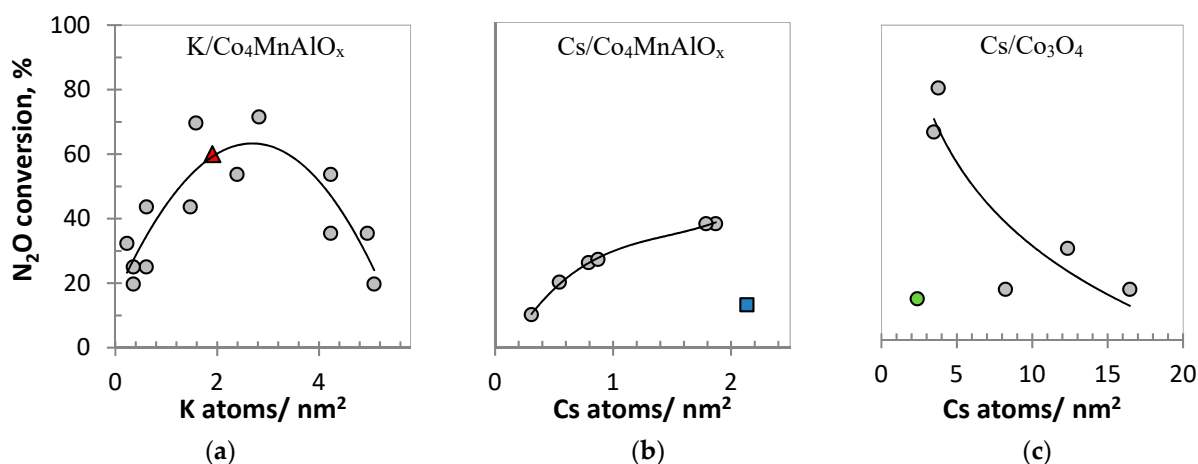

Figure 7. Dependence of N_2O conversion on alkali metal loading. Conditions: 1000 ppm N_2O + 5 mol% O_2 + 2 mol% H_2O in N_2. ⦾ Laboratory prepared catalysts. (**a**) 450 °C, GHSV = 20,000 l kg^{-1} h^{-1}, ▲ K/Co_4MnAlO_x-industry; (**b**) 390 °C, GHSV = 60,000 l kg^{-1} h^{-1}, ■ Cs/Co_4MnAlO_x-industry; (**c**) 330 °C, GHSV = 60,000 l kg^{-1} h^{-1}, ⦾ Cs/Co_3O_4-industry.

It is evident that the conversion of N_2O in the presence of K/Co_4MnAlO_x reaches an optimum at 1.6–2.8 K atoms/nm^2, while in the case of Cs/Co_4MnAl the conversion of N_2O increases with higher Cs loading in the observed concentration range and decreases with increasing Cs loading on Co_3O_4. Loading of K and Cs in samples prepared commercially and in the laboratory are listed in Table 2. In the case of commercially prepared K/Co_4MnAlO_x, the loading of K is in the optimal range, while in

the case of Cs/Co_4MnAlO_x-industry the Cs loading is higher than in the laboratory prepared sample and the dependence of N_2O conversion on Cs loading in this region is unknown. On the contrary, the Cs loading in Cs/Co_3O_4-industry is lower than 3.5, the value that was determined for Cs/Co_3O_4-lab. It is important to mention that the reproducibility of the normalized loading during the preparation was difficult. The reason is that even relatively small changes in the specific surface area and/or the alkali metal content caused a change in the normalized loading, which is already significant due to the relatively narrow optimal range of its value.

The characterization results of laboratory and commercially prepared catalysts showed good correlation with catalytic properties in the kinetic regime:

- The K/Co_4MnAlO_x catalysts demonstrated very similar characteristics for laboratory and commercially prepared samples. Both samples have the same chemical and phase composition; they differ slightly in K content, which is however still in the optimal range, similar to K normalized loading (atoms/nm^2). The samples have the same specific surface areas and crystallite sizes (within the margin of error), which is manifested in also having similar reducibilities.

- The situation is different in the case of Cs-modified catalysts. Here the characterization results differ more significantly, which is reflected by the differences in conversion and kinetic constant values determined in the kinetic regime (Table 1, Figure 3).

- While the commercially prepared Cs/Co_4MnAlO_x has the same chemical and phase composition as the laboratory prepared sample, its crystallite size is 1.8× higher than for the laboratory prepared sample, which leads to both lower specific surface area and worse reducibility. Our previous work proved a direct relationship between the crystallite size and reducibility of Co and Mn in their higher oxidation states (Co^{3+}, Mn^{4+}) in Co_4MnAlO_x [17]. Taking into account that the slowest step of N_2O decomposition is the desorption of oxygen from the catalyst surface connected to the reduction of active sites, worse reducibility of Co^{3+} and probably even Mn^{4+} (corresponding to the temperature maxima of the 1st reduction peak in TPR-H_2) causes a decrease in N_2O conversion. This was observed in the case of the commercially prepared Cs/Co_4MnAlO_x.

- Similarly, the commercially prepared Cs/Co_3O_4 catalyst has the same chemical and phase composition as the laboratory prepared sample. However, the situation regarding crystallite size is completely reversed compared to Cs/Co_4MnAlO_x. The commercially prepared Cs/Co_3O_4 catalyst's crystallite size is 2.7× lower than for the laboratory prepared sample, which corresponds with its higher specific surface area and lower normalized loading of Cs (atoms/nm^2). The reducibility of Co^{3+} and Co^{2+} cannot be determined due to TPR peaks overlapping, but the results indicate different shapes of the cobalt spinel nanocrystals, which affect the catalytic activity [16].

3. Discussion

As determined in Section 2.1, we assume that the *k* value for the K/Co_4MnAlO_x catalyst in the kinetic regime is nearly at its maximum and the increase of N_2O conversion on the tablet catalyst can be theoretically achieved mainly by accelerating the diffusion of reaction mixture molecules in the catalyst's pores. In contrast to this, the increase of N_2O conversion on the Cs/Co_4MnAlO_x and Cs/Co_3O_4 catalysts is possible, besides accelerating internal diffusion, also by optimization of physico-chemical characteristics (crystallite size, reducibility, Cs loading and shape of Co nanocrystals) as described in Section 2.2.

The aim of this part of the paper is to show the limits of increasing conversion by intensification of mass transfer inside pores by tuning the morphology of the catalysts (pore diameter, porosity, and tortuosity) studied for N_2O decomposition.

The measure of reaction rate limitation by internal diffusion is the internal effectiveness factor (Equation (1)). Its dependence on catalyst morphology is represented by the effective diffusion coefficient D_{eff} (Equation (10)), which is influenced by catalyst porosity, tortuosity, and by the ratio of

pore diameter and the reacting molecule's dimension. Table 4 shows the calculated values of the overall diffusivity of N_2O in a multicomponent mixture ($\overline{D}$) according to Equation (11) and the contributions of molecular (D_{mol}) and Knudsen (D_{k,N_2O}) diffusivity according to Equations (12)–(13). The results imply that the prevalent transport mechanism inside pores is Knudsen diffusion, which means that the rate of internal diffusion can be theoretically increased by increasing the pore size and increasing the value of D_k for all three catalysts. In addition, the mass transport inside the pores can be improved by increasing the ε_p/q ratio, i.e. increasing the porosity of the tablets and decreasing the pore tortuosity and thus increasing D_{eff}.
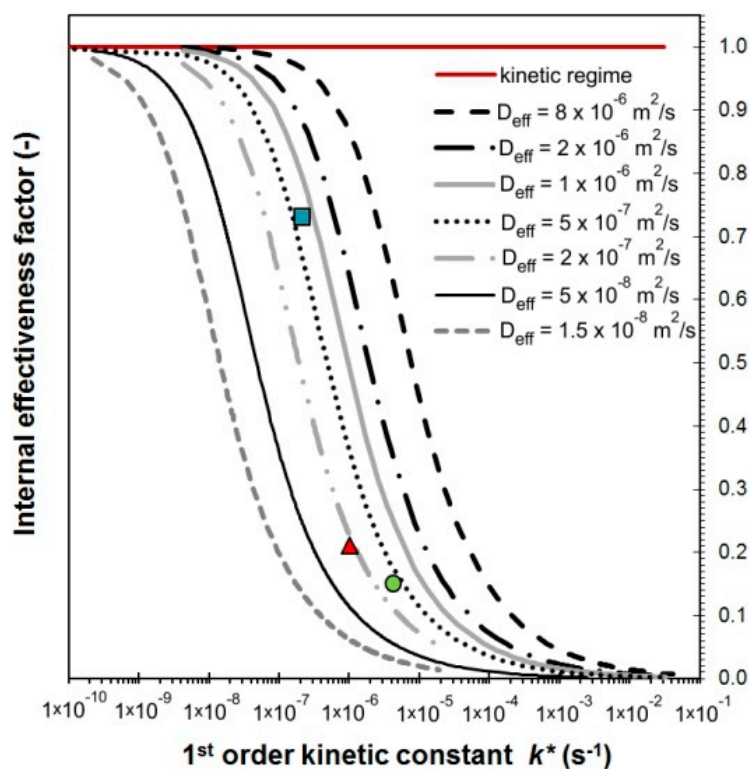

Figure 8. Dependence of internal effectiveness factor on the intrinsic 1st order kinetic constant for different values of effective diffusion coefficients. Calculated for tablets 5.1 mm × 5.1 mm. ▲ K/Co_4MnAlO_x-industry; ■ Cs/Co_4MnAlO_x-industry; ● Cs/Co_3O_4-industry.

Table 4. Diffusion coefficients and tortuosity determined for commercially prepared catalysts. Parameters: 390 °C, 150 kPa, mean pore diameter, model gas mixture 1000 ppm N_2O + 5 mol% O_2 + 2 mol% H_2O in N_2, catalysts in tablets 5.1 mm × 5.1 mm.

Parameter/Catalyst	K/Co_4MnAlO_x-Industry	Cs/Co_4MnAlO_x-Industry	Cs/Co_3O_4-Industry
D_k (m^2 s^{-1})	$2.82 \cdot 10^{-6}$	$4.14 \cdot 10^{-6}$	$1.41 \cdot 10^{-5}$
D_{mol} (m^2 s^{-1})	$7 \cdot 10^{-3}$	$7 \cdot 10^{-3}$	$7 \cdot 10^{-3}$
$\overline{D}$ (m^2 s^{-1})	$2.82 \cdot 10^{-6}$	$4.14 \cdot 10^{-6}$	$1.41 \cdot 10^{-5}$
D_{eff} (m^2 s^{-1}) [1]	$2 \cdot 10^{-7}$	$7.5 \cdot 10^{-7}$	$3.5 \cdot 10^{-7}$
X_{N_2O} model (%) [2]	50	39	85
X_{N_2O} experiment (%) [3]	50	48	88
q [4] (-)	6.78	2.76	18.92
ε_p/q (-)	0.07	0.18	0.02

[1] Determined from Figure 8 for η evaluated from experimental data mentioned in Table 1 [2] Determined from Figure 9 [3] Experimental data of N_2O decomposition over commercial tablets measured in the laboratory at 390 °C and VHSV = 3000 m^3 m$_{bed}$$^{-3}$ h^{-1} (Figure 2) [4] Tortuosity calculated from Equation (10) using experimentally determined porosity (Table 3)
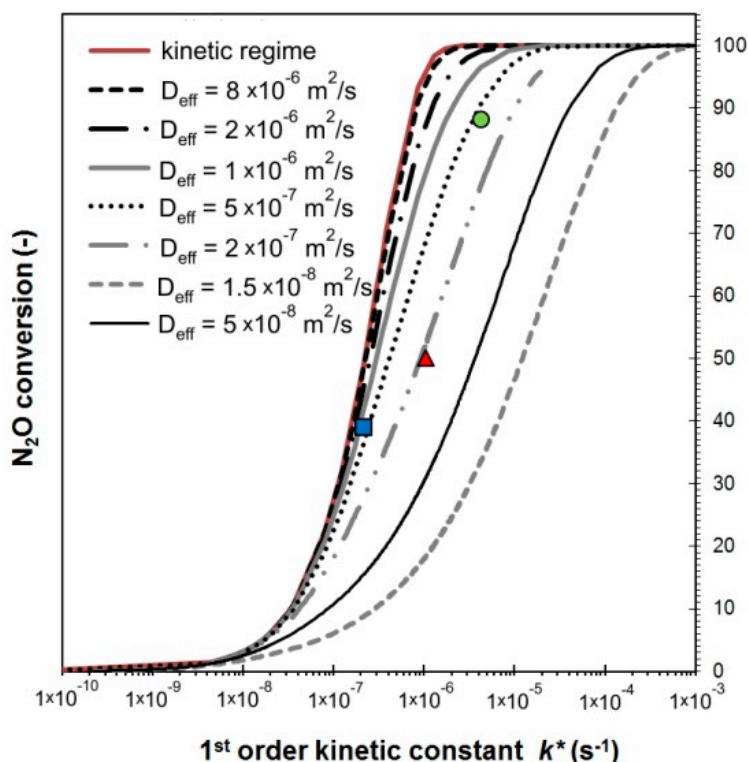
Figure 9. Dependence of theoretically achievable N_2O conversion on the 1st order kinetic constant in kinetic regime. Conversion of N_2O calculated for VHSV = 3000 $m^3.m_{bed}^{-3}.h^{-1}$ and tablets 5.1 mm $\times$ 5.1 mm. ▲ K/Co_4MnAlO_x-industry; ■ Cs/Co_4MnAlO_x-industry; ● Cs/Co_3O_4-industry.

The diagram in Figure 8 shows the dependence of the internal effectiveness factor on the 1st order kinetic constant defined by Equation (4), where η was calculated according to Equations (6)–(8) for different effective diffusion coefficients D_{eff}. Based on the experimentally determined effectiveness factors and intrinsic kinetic constants, the effective diffusion coefficient can be deduced from Figure 8 and then the tortuosity can be calculated using Equation (10). The figure depicts points corresponding to each commercial catalyst. The calculation results for each commercially prepared catalyst are given in Table 4 and the following conclusion can be derived from them:

- The K/Co_4MnAlO_x-industry catalyst has the lowest D_k due to its smallest pores and therefore the lowest overall diffusivity. It also has the second highest tortuosity, which means the second highest ε_p/q ratio (0.07) (the porosity of all catalysts is approximately the same). As a result, it has the lowest effective diffusion coefficient of all three commercial catalysts. Its activity could theoretically be improved via enlargement of pores and lowering their tortuosity, which would lead to an increase of the internal effectiveness factor.
- The Cs/Co_4MnAlO_x-industry has the most favorable morphology for transport because it has the highest effective diffusion coefficient due to the lowest tortuosity and pore size, which is comparable to K/Co_4MnAlO_x-industry. As a result, this catalyst had the highest value of η (0.18) and there is still room to increase its value.

The Cs/Co_3O_4-industry catalyst has the largest pores of all three catalysts, but at the same time the highest tortuosity and thus the least favourable ε_p/q ratio (0.02), resulting in the second highest effective diffusion coefficient. D_{eff} could be further increased by lowering the tortuosity, which would lead to a significantly higher internal effectiveness factor. The diagram in Figure 8 can be used for D_{eff} estimation also for other reactions with 1st order reaction kinetics, when the value of the intrinsic kinetic constant and internal effectiveness factor are known from experiments. The diagram is valid only for shaped catalysts in the form of pellets 5.1 mm $\times$ 5.1 mm or for spheres with diameter of 5.1 mm.

To answer the third question of N_2O conversion limits achievable on tablets by tuning their morphological characteristics, the conversions of N_2O were calculated based on the 1st order intrinsic kinetic constant for different effective diffusion coefficients. The pseudo-homogeneous one-dimensional model of an ideal plug flow reactor in an isothermal regime, mentioned in our previous paper [12], was used for the calculation, where the effect of internal and external mass transport was described by the overall effectiveness factor Ω. Considering that the resistance to mass transfer by internal diffusion is prevalent, the overall effectiveness factor was substituted by the internal effectiveness factor, which was incorporated into the 1st order kinetic equation $r = \eta\, k\, c_A$. This model disregards pressure drop.

In Table 4, the calculated N_2O conversions for VHSV = 3000 $m^3.m_{bed}^{-3}.h^{-1}$ and catalyst tablets 5.1 mm $\times$ 5.1 mm are compared with experimental N_2O conversions determined at the same VHSV (Figure 2), and quite good agreement between the X_{N_2O} model and X_{N_2O} experiment was reached. The diagram showing the dependence of theoretically reachable N_2O conversion on the 1st order kinetic constant in the kinetic regime is shown in Figure 9. The dependencies imply that the catalyst with a higher kinetic constant in the kinetic regime after tabletization can demonstrate lower N_2O conversion than a sample which is less active in the kinetic regime, but has a more favorable tablet texture (pore size, porosity, and tortuosity). The figure depicts points corresponding to each commercial catalyst calculated according to reactor model. Their placement implies that the activity of the Cs/Co_4MnAlO_4-industry catalyst (39% N_2O conversion) cannot be further increased by much; since a N_2O conversion of 50% corresponds to kinetic regime. The situation is similar for the Cs/Co_3O_4-industry catalyst, which reaches 90% conversion under the given conditions, while the conversion corresponding to the kinetic regime is 100%. On the other hand, there is a relatively large room for improvement of N_2O conversion on the K/Co_4MnAlO_x-industry sample (50% conversion) since a N_2O conversion of 95% corresponds to the kinetic regime.

4. Materials and Methods

4.1. Preparation of Catalysts at Laboratory Scale

4.1.1. K/Co_4MnAlO_x and Cs/Co_4MnAlO_x

The Co-Mn-Al layered double hydroxide (LDH) precursor with Co:Mn:Al molar ratio of 4:1:1 was prepared by co-precipitation of the corresponding nitrates in $Na_2CO_3/NaOH$ solution at 25 °C and pH 10. The product was washed and dried at 60 °C and then calcined for 4 h at 500 °C in air. The prepared mixed oxide was then crushed and sieved to obtain a fraction with particle size of 0.160–0.315 mm. The next step in preparation was impregnation by the pore filling method using aqueous solutions of KNO_3 or Cs_2CO_3 to obtain a K content of 1.8 wt% and Cs content of 4 wt%, respectively. The dried products were calcined for 4 h at 500 °C in air, sieved to obtain a fraction with particle size of 0.160–0.315 mm and marked as K/Co_4MnAlO_x-lab and Cs/Co_4MnAlO_x-lab.

4.1.2. Cs/Co_3O_4

$Co(NO_3)_2 \cdot 6H_2O$ was added to an NaOH solution at room temperature while stirring. The concentration of the alkaline solution was chosen to maintain the required molar ratio of OH to Co in the reaction mixture. The resulting suspension was maintained under stirring with air bubbling at room temperature for 5 minutes. Subsequently, the solid product was filtered, washed with distilled water, and dried at 30 °C. The dried products were calcined for 4 h at 500 °C in air and sieved to obtain a fraction with a particle size of 0.160–0.315 mm. The next step in preparation was impregnation by the pore filling method using aqueous solutions of Cs_2CO_3 to obtain Cs content of 1wt%. The dried products were calcined for 4 h at 500 °C in air, sieved to obtain a fraction with particle size of 0.160–0.315 mm and marked as Cs/Co_3O_4-lab.

4.2. Preparation of Catalysts on Large Scale

4.2.1. K/Co$_4$MnAlO$_x$ and Cs/Co$_4$MnAlO$_x$

The Co−Mn−Al LDH with Co:Mn:Al molar ratio of 4:1:1 was used as a precursor of Co$_4$MnAlO$_x$ mixed oxide and was prepared by co-precipitation of the corresponding nitrates in an alkaline Na$_2$CO$_3$/NaOH solution at 25 °C and pH 10. Concentrations of 40 and 106 mol/l were used for NaOH and Na$_2$CO$_3$, respectively. The resulting suspension was filtered off, washed with water, dried at 60–105 °C, and calcined for 4 h at 500 °C in air. The resulting product was milled, impregnated with KNO$_3$ or Cs$_2$CO$_3$ to obtain K content of 1.8wt% and Cs content of 4wt%, respectively, calcined (4 h, 500 °C) and shaped into tablets (5 mm × 5 mm). For better shaping, graphite was added. The catalyst was produced by ASTIN Catalysts and Chemicals, Ltd., Litvínov, Czech Republic and marked as K/Co$_4$MnAlO$_x$-industry and Cs/Co$_4$MnAlO$_x$-industry.

4.2.2. Cs/Co$_3$O$_4$-industry

The Co(OH)$_2$−β was used as a precursor of Co$_3$O$_4$ and was prepared by co-precipitation of cobalt nitrates in an alkaline NaOH solution at 25 °C. The resulting suspension was filtered off, washed with water, dried at 60 °C and calcined for 4 h at 500 °C in air. The resulting product was milled, impregnated with Cs$_2$CO$_3$ to obtain Cs content of 1 wt%, dried, calcined (4 h at 500 °C) and shaped into tablets (5 mm × 5 mm). For better shaping, graphite was added. The catalyst was produced by ASTIN Catalysts and Chemicals, Ltd., Litvínov, Czech Republic and marked as Cs/Co$_3$O$_4$.

4.3. Characterization of Catalysts

The chemical composition of samples was determined by atomic absorption spectrometry or atomic emission spectrometry using a SpectrAA880 instrument (Varian, Palo Alto, CA, USA) after dissolving the samples in hydrochloric acid.

Phase composition and microstructural properties were determined using the X-ray powder diffraction (XRD) technique. XRD patterns were obtained using a Rigaku SmartLab diffractometer (Rigaku, Tokio, Japan) with D/teX Ultra 250 detector. The source of X-ray irradiation was Co tube (CoKα, λ_1 = 0.178892 nm, λ_2 = 0.179278 nm) operated at 40 kV and 40 mA. Incident slits were set up to irradiate a 10 mm × 10 mm area of the sample (automatic divergence slits) constantly. The XRD patterns were collected in a 2θ range 5–90° with a step size of 0.01° and speed 0.5 deg.min^{-1}. The samples were rotated (30 rpm) during the measurement. Lattice parameters were refined using the LeBail method; the sizes of coherent domains were calculated using Scherrer's formula as an average of the five strongest diffractions with hkl symbols (220), (311), (400), (511), and (440) evaluated.

The surface areas of the catalysts were determined by N$_2$ adsorption/desorption at −196 °C using the ASAP 2010 instrument (Micromeritics, Ottawa, Ontario, Canada) and evaluated by the Brunauer–Emmett–Teller (BET) method. Prior to the measurement, both laboratory and commercially prepared samples were crushed to obtain a fraction <0.16 mm and dried at 120 °C for at least 12 h.

In addition, textural properties of the commercially prepared catalysts were determined using the 3Flex physisorption set-up (Micromeritics, Ottawa, Ontario, Canada) and pieces of catalyst tablets were used for measurements. Before the physisorption measurement, the samples were dried at 120 °C for 12 h in vacuum. The nitrogen adsorption–desorption isotherms were measured at 77 K. The specific surface area, S_{BET}, was calculated based on the BET method. The mesopore surface area, S_{meso}, and the micropore volume, V_{micro}, were evaluated by using the t-plot method, applying the Broekhoff-de-Boer standard isotherm. The total pore volume, V_{net}, was evaluated as the nitrogen volume adsorbed at maximum relative pressure (p/p_0 = 0.99). The pore-size distribution was evaluated from adsorption data applying the Barrett-Joyner-Halenda (BJH) method, assuming cylindrical pore geometry and using the Broekhoff-de-Boer standard isotherm with Faas correction.

The porous structure (mesopores and macropores) of commercial catalysts was characterized using a mercury porosimeter AutoPore III (Micromeritics, Ottawa, Ontario, Canada) working in the

range of 0.1–400 MPa. Prior to the measurement, the samples were dried at 130 °C. Helium pycnometry (AccuPyc1330, Micrometrics, Ottawa, Ontario, Canada) was used to evaluate the sample's true density.

Temperature programmed reduction (H_2-TPR) measurements of the calcined samples (0.025 g) were performed using a system described in detail in [21], with a H_2/N_2 mixture (10 mol% H_2), flow rate 50 ml/min and linear temperature increase of 20 °C/min up to 1000 °C. The change in H_2 concentration was evaluated using an Omnistar 300 mass spectrometer (Pfeiffer Vacuum, Asslar, Germany).

4.4. Catalytic Tests on Laboratory Scale

Catalytic experiments for laboratory prepared catalysts and crushed pellets with particle size 0.165–0.315 mm were performed in a reactor with an internal diameter of 5.5 mm. A catalytic bed contained 0.1–0.3 g of the sample; the total flow rate was 100 ml/min (20 °C, 101,325 Pa) containing 0.1 mol% N_2O, 5 mol% O_2 and 2 mol% water vapor in N_2 leading to GHSV = 20,000–60,000 l $kg^{-1}h^{-1}$ was applied to simulate the real waste gas from a nitric acid plant.

Experiments with commercially prepared pellets were performed in an integral reactor with an internal diameter of 50 mm. The catalytic bed contained 10 ml of the sample, the total flow rate was 500 ml/min (20 °C, 101,325 Pa) containing 0.1 mol% N_2O, 5 mol% O_2 and 2 mol% water vapor in N_2 to simulate the real waste gas from a nitric acid plant. VHSV = 3000 m^3 m_{bed}^{-3} h^{-1} was applied.

4.5. Pilot Plant Catalytic Tests

Pilot plant catalytic measurements of N_2O decomposition were performed in a fixed bed stainless steel reactor (0.31 m internal diameter) in the temperature range of 350 to 450 °C and inlet pressure of 0.6 MPa. The reactor was connected to the bypassed tail gas from the nitric acid production plant downstream from the SCR NO_x/NH_3 catalyst. The catalyst tablets (K/Co_4MnAlO_x-industry: 69.1 kg weight, 62.5 cm bed height, 1334 kg m^{-3} bed density; Cs/Co_4MnAlO_x-industry: 74.4 kg weight, 62.5 cm bed height, 1436 kg m^{-3} bed density; Cs/Co_3O_4-industry: 75.9 kg weight, 60 cm bed height, 1527 kg m^{-3} bed density) were placed on a stainless steel grate sieve and a bed of ceramic spheres (diameter of 8 mm) 5 cm in height. On the catalyst layer, again more ceramic spheres (height of 1 cm), a sieve, and a last layer of ceramic spheres (height of 6.5 cm) were placed. The feed to the reactor varied between 300 and 600 kg h^{-1} and contained typically 400−700 ppm of N_2O together with oxygen, water vapor, and a low concentration of NO, NO_2, and NH_3 (0−70 ppm of NO_x, 0−30 ppm of NH_3). The variable composition of gas mixture at the reactor inlet was due to the fact that the inlet gas was the real waste gas from the nitric acid plant downstream from the SCR NO_x/ NH_3 unit. Infrared and chemiluminescence online analyzers were used for analysis of the gas at the catalyst bed inlet and outlet: Sick (N_2O), Horiba (NO, NO_2), ABB modul Uras 26 (N_2O), and ABB Limas11 (NO, NO_2, and NH_3). The reactor was equipped with online monitoring of the concentrations of all measured gas components, the temperature in the catalyst bed, and the pressure drop.

4.6. Determination of Internal Effectiveness Factor

The internal effectiveness factor expresses the influence of the internal mass transport limitation on the overall rate of catalytic reaction and is defined by Equation (1).

$$\eta = \frac{Actual\ overall\ rate\ of\ reaction}{Rate\ of\ reaction\ that\ would\ result\ if\ entire\ interior\ was\ exposed\ to\ external\ pellet\ surface\ conditions} \tag{1}$$

Both the experimental determination and the theoretical calculation of η were used. For the determination from experimental data, N_2O conversions at the same reaction conditions had to be used for evaluation of both reaction rates in Equation (1). We assume that the rate of reaction on the catalyst in the form of grains is not affected by internal diffusion and can be used as the reaction

rate at external pellet surface conditions. For the evaluation of the actual overall rate of reaction, N_2O conversions over pellets were recalculated to the same GHSV which was used for the testing of grains (GHSV = 60,000 l h^{-1}kg^{-1} = 0.00025 m^{3}s^{-1}kg^{-1}) using 1st order kinetic equation and the material balance of an ideal plug flow reactor:

$$X_{N_2O} = 1 - e^{\frac{-k}{GHSV}} \tag{2}$$

Kinetic constants over catalyst pellets and grains were calculated from N_2O conversions according to Equations (3) and (4):

$$k = \frac{\ln\left(\frac{1}{1-X_{N_2O}}\right)}{\frac{w}{\dot{V}}} \tag{3}$$

$$k^* = k/\rho_c \tag{4}$$

where k (m^3 s^{-1} kg^{-1}) and k^* (s^{-1}) are 1st order kinetic constants, w (kg) is the weight of catalyst, $\dot{V}$ (m^3 s^{-1}) the total gas flow and ρ_c (kg m^{-3}) is the bulk density of catalyst determined by Hg porosimetry. Then both reaction rates, defined as the amount of N_2O converted per kg of catalysts per hour (mol$_{N2O}$ kg$_{cat}$$^{-1}$ h^{-1}), were calculated (r_{grain} and r_{pellet}, respectively). The ratio of r_{grain}/r_{pellet} provides the internal effectiveness factor of the pellets utilization.

$$r = k \cdot c_{A0} \cdot (1 - X_{N_2O}) \tag{5}$$

where X_{N_2O} is N_2O conversion (-), c_{A0} inlet N_2O concentration (mol m^{-3}).

For the theoretical estimation of the internal effectiveness factor η for catalyst pellets, Equations (6)–(13) were used [22].

$$\eta = \frac{1}{\Phi_{gen}} \cdot tanh\ \Phi_{gen} \quad \text{for } \Phi gen\ < \ 4 \tag{6}$$

$$\eta = \frac{1}{\Phi_{gen}} \quad \text{for } \Phi gen\ > \ 4 \tag{7}$$

where the generalized Thiele modulus Φ_{gen} is defined:

$$\Phi_{gen} = \frac{V}{S} \cdot \sqrt{\frac{k \cdot \rho_c}{D_{eff}}} \tag{8}$$

where for cylinder pellet with equal diameter and height ($d_p = h$):

$$\frac{V}{S} = \frac{d_p}{6} \tag{9}$$

The effective diffusion coefficient D_{eff} is dependent on the morphology of porous catalyst:

$$D_{eff} = \frac{\varepsilon_p}{q}\overline{D} \tag{10}$$

The ε_p/q ratio between 0.05–0.1 was published previously [23]. For the determination of the overall diffusivity of N_2O in a multicomponent mixture ($\overline{D}$), the contributions of molecular ($D_{i/j}$) and Knudsen (D_{k,N_2O}) diffusivity was considered together with the stoichiometry of the reaction [12]:

$$\frac{1}{\overline{\overline{D}}} = \frac{1}{D_{k,N_2O}} + \frac{x_{N_2O} + x_{N_2O}}{D_{\frac{N_2O}{N_2}}} + \frac{0.5 \cdot x_{N_2O} + 0.5 \cdot x_{N_2O}}{D_{\frac{N_2O}{O_2}}} + \sum_{j=1}^{n} \frac{x_{N_2O}}{D_{N_2O/j}} \tag{11}$$

where j is a component of gas mixture. The Knudsen diffusivity D_{k,N_2O} for pore with radius r_o was determined [23] as:

$$D_{k,N_2O} = 97 \cdot r_o \cdot \sqrt{\frac{T}{M_{N_2O}}} \tag{12}$$

Binary diffusion coefficients $D_{i/j}$ were calculated from Equation (13) [24]:

$$D_{i/j} = \frac{\frac{10^{-2} \cdot T^{\frac{7}{4}} \cdot \left(M_j^{-1} + M_i^{-1}\right)^{\frac{1}{2}}}{p}}{\left[(\sum v)_i^{\frac{1}{3}} + (\sum v)_j^{\frac{1}{3}}\right]^2} \tag{13}$$

where $(\sum v)_{N_2} = 17.9$, $(\sum v)_{N_2O} = 35.9$, $(\sum v)_{O_2} = 16.6$, $(\sum v)_{H_2O} = 12.7$, $(\sum v)_{He} = 2.88$, $(\sum v)_{NO} = 11.17$.

5. Conclusions

Three cobalt containing mixed oxides modified with alkali metal promoters (K/Co_4MnAlO_x, Cs/Co_4MnAlO_x and Cs/Co_3O_4) were prepared commercially in the form of tablets. Their catalytic properties were tested for N_2O catalytic decomposition in the laboratory and in a pilot plant reactor connected to the waste gas from a nitric acid production plant and compared to the laboratory prepared catalysts with the same chemical composition.

It was found that the different order of catalytic activities in the pilot-plant experiment compared to the laboratory prepared catalysts was caused by the different conditions of the pilot plant experiment, particularly by the presence of NO_x and NH_3.

Comparison of N_2O conversions of both laboratory and commercially prepared catalysts in the kinetic regime showed that K/Co_4MnAlO_x has active sites with nearly the same activity as the laboratory prepared sample and the kinetic constant of the tablets is lower mainly due to the inhibiting effect of internal diffusion. N_2O conversion in such a case can be improved by increasing the internal effectiveness factor, i.e. by increasing D_{eff}, which can be achieved by increasing the pore size and also by increasing porosity and decreasing tortuosity.

Conversely, commercially prepared Cs/Co_4MnAlO_x and Cs/Co_3O_4 catalysts possess active sites which are less active than those of laboratory prepared catalysts. N_2O conversions on these tablets were lower partly due to the inhibiting effect of internal diffusion and also due to observed differences in reducibility, primary particle sizes, and probably also promoter normalized loading (atoms/nm^2) compared to laboratory prepared catalysts of the same chemical composition. N_2O conversion on such tablets can be increased mainly by optimizing the preparation procedure and increasing the activity of the active sites (by increasing k).

The shown dependencies answer the question from the title of the paper: It is possible that a catalyst with a great performance in the kinetic regime can be less effective when prepared commercially in the form of tablets. The major reason for such changes in catalyst activity order after scale up are morphological characteristics (limiting mass transfer rates) and for that reason these can sometimes be even more important than the catalyst composition itself.

Symbols

a	lattice parameter (nm)
c_A	concentration of component A (N_2O) (mol.m^{-3})
c_{A0}	initial concentration of component A (N_2O) (mol.m^{-3})
$\overline{D}$	overall diffusivity (m$_2$.s^{-1})
D_{eff}	effective diffusion coefficient (m^2.s^{-1})
D_{ij}	binary diffusion coefficient of molecular diffusivity (m^2.s^{-1})
D_k	Knudsen diffusivity (m^2.s^{-1})
d_p	equal catalyst particle diameter (m)
k	kinetic constant, 1st order rate law (m^{3}s^{-1}kg^{-1})
$k*$	kinetic constant, 1st order rate law (s^{-1})
L_c	size of coherent domains
M_i	molar weight of compound i (g.mol^{-1})
q	tortuosity (-)
r	reaction rate per unit weight of catalyst (mol.kg^{-1}.h^{-1})
r_o	catalyst pore radius (m)
S_{BET}	specific surface area (m^2 g^{-1})
V	volume of the catalyst bed (m^3)
$\dot{V}$	total volumetric flow (m^3 s^{-1})
V_{net}	total pore volume (cm$^3_{liq}$ g^{-1})
v_i	molar volume of component i (m^3.kmol^{-1})
w	catalyst weight (g)
X_A	conversion of component A (N_2O) (-)
x_{N2O}	molar fraction of N_2O entering the reactor (-)

Greek symbols:

ε_p	porosity of catalyst particle (-)
Φ_{gen}	generalized Thiele modul (-)
η	internal effectiveness factor (-)
ρ_c	bulk density of the catalyst (kg.m^{-3})

References

1. Chromčáková, Ž.; Obalová, L.; Kustrowski, P.; Drozdek, M.; Karásková, K.; Jirátová, K.; Kovanda, F. Optimization of Cs content in Co–Mn–Al mixed oxide as catalyst for N_2O decomposition. *Res. Chem. Intermed.* **2015**, *41*, 9319–9332. [CrossRef]

2. Obalová, L.; Karásková, K.; Jirátová, K.; Kovanda, F. Effect of potassium in calcined Co–Mn–Al layered double hydroxide on the catalytic decomposition of N_2O. *Appl. Catal. B Environ.* **2009**, *90*, 132–140. [CrossRef]

3. Lucie Obalová, S.M. Cesium doped Co_3O_4 spinel for N_2O decomposition. In Proceedings of the 5th International Conference on Chemical Technology, Mikulov, Czech Republic, 10–12 April 2017.

4. Pacultová, K.; Karásková, K.; Kovanda, F.; Jirátová, K.; Šrámek, J.; Kustrowski, P.; Kotarba, A.; Chromčáková, Ž.; Kočí, K.; Obalová, L. K-Doped Co–Mn–Al Mixed Oxide Catalyst for N_2O Abatement from Nitric Acid Plant Waste Gases: Pilot Plant Studies. *Ind. Eng. Chem. Res.* **2016**, *55*, 7076–7084. [CrossRef]

5. Pacultová, K.; Chromčáková, Ž.; Obalová, L. Cs doped cobalt based deN_2O catalyst-Pilot plant results. *Waste Forum* **2017**, *2*, 54–63.

6. Inger, M.; Kowalik, P.; Saramok, M.; Wilk, M.; Stelmachowski, P.; Maniak, G.; Granger, P.; Kotarba, A.; Sojka, Z. Laboratory and pilot scale synthesis, characterization and reactivity of multicomponent cobalt spinel catalyst for low temperature removal of N_2O from nitric acid plant tail gases. *Catal. Today* **2011**, *176*, 365–368. [CrossRef]

7. Inger, M.; Wilk, M.; Saramok, M.; Grzybek, G.; Grodzka, A.; Stelmachowski, P.; Makowski, W.; Kotarba, A.; Sojka, Z. Cobalt Spinel Catalyst for N_2O Abatement in the Pilot Plant Operation–Long-Term Activity and Stability in Tail Gases. *Ind. Eng. Chem. Res.* **2014**, *53*, 10335–10342. [CrossRef]

8. Obalová, L.; Karásková, K.; Wach, A.; Kustrowski, P.; Mamulová-Kutláková, K.; Michalik, S.; Jirátová, K. Alkali metals as promoters in Co–Mn–Al mixed oxide for N_2O decomposition. *Appl. Catal. A Gen.* **2013**, *462–463*, 227–235.

9. Karásková, K.; Obalová, L.; Jirátová, K.; Kovanda, F. Effect of promoters in Co–Mn–Al mixed oxide catalyst on N_2O decomposition. *Chem. Eng. J.* **2010**, *160*, 480–487. [CrossRef]

10. Yamada, K.; Pophal, C.; Segawa, K. Selective catalytic reduction of N_2O by C_3H_6 over Fe-ZSM-5. *Microporous Mesoporous Mater.* **1998**, *21*, 549–555. [CrossRef]

11. Chmielarz, L.; Kuśtrowski, P.; Rafalska-Łasocha, A.; Dziembaj, R. Selective oxidation of ammonia to nitrogen on transition metal containing mixed metal oxides. *Appl. Catal. B Environ.* **2005**, *58*, 235–244. [CrossRef]

12. Obalová, L.; Jirátová, K.; Karásková, K.; Chromčáková, Ž. N_2O catalytic decomposition – From laboratory experiment to industry reactor. *Catal. Today* **2012**, *191*, 116–120. [CrossRef]

13. Pasha, N.; Lingaiah, N.; Babu, N.S.; Reddy, P.S.S.; Prasad, P.S.S. Studies on cesium doped cobalt oxide catalysts for direct N_2O decomposition in the presence of oxygen and steam. *Catal. Commun.* **2008**, *10*, 132–136. [CrossRef]

14. Stelmachowski, P.; Maniak, G.; Kotarba, A.; Sojka, Z. Strong electronic promotion of Co_3O_4 towards N_2O decomposition by surface alkali dopants. *Catal. Commun.* **2009**, *10*, 1062–1065. [CrossRef]

15. Galejová, K.; Obalová, L.; Jiratova, K.; Pacultová, K.; Kovanda, F. N_2O catalytic decomposition—Effect of pelleting pressure on activity of Co-Mn-Al mixed oxide catalysts. *Chem. Pap.* **2009**, *63*, 172–179. [CrossRef]

16. Gudyka, S.; Grzybek, G.; Gryboś, J.; Indyka, P.; Leszczyński, B.; Kotarba, A.; Sojka, Z. Enhancing the deN_2O activity of the supported $Co_3O_4 | \alpha$-Al_2O_3 catalyst by glycerol-assisted shape engineering of the active phase at the nanoscale. *Appl. Catal. B Environ.* **2017**, *201*, 339–347. [CrossRef]

17. Klyushina, A.; Pacultová, K.; Karásková, K.; Jirátová, K.; Ritz, M.; Fridrichová, D.; Volodarskaja, A.; Obalová, L. Effect of preparation method on catalytic properties of Co-Mn-Al mixed oxides for N_2O decomposition. *J. Mol. Catal. A Chem.* **2016**, *425*, 237–247. [CrossRef]

18. Kaczmarczyk, J.; Zasada, F.; Janas, J.; Indyka, P.; Piskorz, W.; Kotarba, A.; Sojka, Z. Thermodynamic Stability, Redox Properties, and Reactivity of Mn_3O_4, Fe_3O_4, and Co_3O_4 Model Catalysts for N_2O Decomposition: Resolving the Origins of Steady Turnover. *ACS Catal.* **2016**, *6*, 1235–1246. [CrossRef]

19. Obalová, L.; Maniak, G.; Karásková, K.; Kovanda, F.; Kotarba, A. Electronic nature of potassium promotion effect in Co–Mn–Al mixed oxide on the catalytic decomposition of N_2O. *Catal. Commun.* **2011**, *12*, 1055–1058. [CrossRef]

20. Maniak, G.; Stelmachowski, P.; Zasada, F.; Piskorz, W.; Kotarba, A.; Sojka, Z. Guidelines for optimization of catalytic activity of 3d transition metal oxide catalysts in N_2O decomposition by potassium promotion. *Catal. Today* **2011**, *176*, 369–372. [CrossRef]

21. Jirátová, K.; Mikulová, J.; Klempa, J.; Grygar, T.; Bastl, Z.; Kovanda, F. Modification of Co–Mn–Al mixed oxide with potassium and its effect on deep oxidation of VOC. *Appl. Catal. A Gen.* **2009**, *361*, 106–116. [CrossRef]

22. Fogler, H.S. *Elements of Chemical Reaction Engineering*, 3rd ed.; Prentice Hall PTR: Upper Saddle River, NJ, USA, 1999.

23. Kaptejn, F.; Moulijn, J.A. *Handbook of Heterogeneous Catalysis*; Ertl, G., Knözinger, H., Weitkamp, J., Eds.; Wiley: Weinheim, Germany, 1996.

24. Fuller, E.N.; Schettler, P.D.; Giddings, J.C. New method for prediction of binary gas-phase diffusion coefficients. *Ind. Eng. Chem.* **1966**, *58*, 18–27. [CrossRef]